Measurement 69 (2015) 9–19

Contents lists available at ScienceDirect

Measurement

journal homepage: www.elsevier.com/locate/measurement

Study on Single-bin Sliding DFT algorithms: Comparison, stability issues and frequency adaptivity

Carlos M. Orallo [*,1], Ignacio Carugati [1], Patricio G. Donato [1], Sebastian Maestri [1]

Universidad Nacional de Mar del Plata, Facultad de Ingeniería, Laboratorio de Instrumentación y Control, Juan B. Justo 4302, Mar del Plata, Argentina

ARTICLE INFO

Article history:
Received 20 October 2014
Received in revised form 9 February 2015
Accepted 10 March 2015
Available online 19 March 2015

Keywords:
Power quality
Harmonics measurement
System modeling
Discrete Fourier transform
Digital signal processing
Control design

ABSTRACT

The standard method for spectrum analysis is the Discrete Fourier Transform(DFT), typically implemented using a Fast Fourier Transform (FFT) algorithm. However, certain applications require an on-line spectrum analysis only on a subset of M frequencies of an N-point DFT ($M < N$). In such cases, the use of Single-bin Sliding DFT (Sb-SDFT) is preferred over the direct application of FFT. Along these lines, the most popular algorithms are the Sliding Discrete Fourier Transform (SDFT), the Sliding Goertzel Transform (SGT), the Modulated Sliding Discrete Fourier Transform (mSDFT), and the S. Douglas and J. Soh algorithm (D&S). Even though these methods seem to differ, they are derived from the conventional DFT using distinct approaches and properties. To better understand the advantages, limitations and similarities each of them have, this work thoroughly evaluates and compares the four Sb-SDFT methods. What is more, the direct application of these Sb-SDFTs may lead to inaccuracies due to spectral leakage and picket-fence effects, common pitfalls inherited by every DFT-based method. For this reason, a unified model of the Sb-SDFT methods is proposed, whose aim is to design a frequency adaptive control loop. This frequency adaptability allows to mitigate the problems associated with improper sampling frequency. By using this unified model, the election of the Sb-SDFT algorithm is independent of the controller design and all the methods are equivalent. Theoretical results are validated by simulations and a DSP implementation of the four frequency adaptive Single-bin Sliding DFT methods.

1. Introduction

The proliferation of advanced power electronic technologies, such as switching power supplies and adjustable speed motor drives, among others, have led to an increment in the harmonic currents injected into power systems, causing power quality degradation. Harmonic pollution can cause serious problems in power systems, e.g., it can accentuate losses in distribution networks and rotating machines, lead to inaccurate operation of protection and control systems, damage sensitive loads and create significant interference in communication systems. In addition, the system frequency may deviate from its nominal value due to the imbalance between power generation and load demand. Therefore, interest lies in measuring the harmonic components of non-stationary signals, such as grid voltage and currents for grid monitoring and implementation of preventive strategies [1–3].

Various approaches estimate the harmonic content of electrical signals. The method most commonly used is the Discrete Fourier Transform (DFT), implemented by the Fast Fourier Transform (FFT) [4–6] due to its computational efficiency. By transforming the measured signal

* Corresponding author.
E-mail address: orallo@fi.mdp.edu.ar (C.M. Orallo).
[1] The authors are with the Universidad Nacional de Mar del Plata, CONICET.

http://dx.doi.org/10.1016/j.measurement.2015.03.011
0263-2241/

from the time domain to the frequency domain, FFT can accurately track its harmonic components.

For some real-time applications, the direct application of conventional DFT methods or more efficient FFT techniques can be complex and/or involve an excessive computational cost. However, certain applications require an on-line spectrum analysis only over a subset of M frequencies of an N-point DFT ($M < N$). For this scenario, the common practice is to utilize Single-bin Sliding DFT algorithms (Sb-SDFT). These algorithms efficiently calculate a unique spectral component of an N-point DFT. The Sliding Discrete Fourier Transform (SDFT) [7,8], the Sliding Goertzel Transform (SGT) [9,10], the Modulated Sliding Discrete Fourier Transform (mSDFT) [11] and the S. Douglas and J. Soh algorithm (D&S) [12] are among the most popular Sb-SDFT methods. These four techniques have spectral bin output rates equal to the input data rate on a sample-by-sample basis.

Nonetheless, since the harmonic level and the fundamental frequency in the power system are usually time-varying, the direct application of DFT-based methods for spectral analysis may lead to inaccuracies due to spectral leakage and picket-fence effects [13]. These unwanted effects are related to the frequency variation and improperly selected sampling time window. In order to solve this problem, the authors present in [14] a harmonic measurement method which employs the mSDFT algorithm and a frequency adaptive mechanism. This mechanism, named Variable Sampling Period Technique (VSPT), dynamically adjusts the sampling period to exactly N times the fundamental frequency, thereby avoiding the above-mentioned problems.

Despite the fact that Sb-SDFT methods seem to be different, they are derived from the conventional DFT with distinct approaches and properties. Thus they bear great similarities that are frequently overlooked. This paper evaluates and compares the four selected Sb-SDFT algorithms in diverse operational conditions, identifying the similarities between them. Based on this analysis, a unified mathematical model is proposed for the implementation of VSPT in order to achieve a frequency adaptive system. The purpose of obtaining a unified model is to make the choice of an Sb-SDFT independent from the design of the control in charge of frequency adjustment, rendering the design and implementation process more flexible and convenient. Moreover, it allows to change the algorithm without redesigning the control loop. By using the unified model proposed here, the benefits of this frequency adaptive mechanism can be extrapolated to all the algorithms discussed in this manuscript. The model obtained, together with its usefulness in the design process, is validated by experimental results obtained in a DSP platform.

The paper is organized as follows: Section 2 presents a brief review of Sb-SDFT. The steady-state characteristics of the reviewed methods are analyzed in Section 3, while their dynamic behaviors are presented in Section 4. In Section 5, a scheme for frequency adaptation (VSPT) to mitigate the inaccuracies resulting from the spectral leakage and picket-fence effect is introduced. A unified model is presented to generalize this scheme to all Sb-SDFT along with simulation results. The experimental results for the implementation of the reviewed Sb-SDFT with VSPT, based on the unified model, are shown in Section 6. Finally, the conclusions of this work are drawn in Section 7.

2. Review of Single-bin Sliding Discrete Fourier Transforms

The standard method for spectrum analysis in digital signal processing is the Discrete Fourier Transform (DFT). DFT converts a finite series of equally spaced samples of a function into a series of coefficients of a finite combination of complex sinusoids, ordered by their frequencies. Therefore, DFT converts the sampled function from its original time domain to the frequency domain.

The DFT of the sequence $x(n)$ is defined as

$$X(k) = \sum_{n=0}^{N-1} x(n) W_N^{-kn} \tag{1}$$

where $X(k)$ is the DFT output coefficient, $W_N = e^{j2\pi/N}$ is the complex twiddle factor, N is the sequence length, k is the frequency domain index ($0 \leqslant k \leqslant N-1$) and n is the time domain index [4].

For a number of real-time applications, the direct application of conventional DFT methods can be complex and demand high computational effort. Additionally, there are applications that require spectrum analysis only over a subset of M frequencies of an N-point DFT. In such instances, it is convenient to use a Single-bin Sliding Discrete Fourier Transform (Sb-SDFT) algorithm, which computes a single complex DFT spectral bin value by means of a sliding window.

One of the most common Sb-SDFTs, is the Sliding Discrete Fourier Transform (SDFT). SDFT is a recursive algorithm that performs an N-point DFT on time samples within a sliding window on a sample-by-sample basis. The time window is advanced one sample at a time, and a new N-point DFT is calculated. The principle used for SDFT is known as the DFT shifting theorem, or the circular shift property.

SDFT can be recursively implemented to calculate Eq. (1) for a desired k-bin, as:

$$X_k(n) = W_N^k X_k(n-1) - x(n-N) + x(n) \tag{2}$$

where $X_k(n)$ is calculated by phase shifting the sum of the previous $X_k(n-1)$ with the difference between the current and delayed input sample, $x(n)$ and $x(n-N)$, respectively [7,8].

SDFT is computationally efficient, as it only requires one (complex) multiplication and two additions per time instant. Nevertheless, the implementation of Eq. (2) as an IIR filter in a system with finite word-length precision brings about a rounding error in the implementation of the W_N^k coefficient, resulting in accumulated errors and potential instabilities. The latter is explained by wrong cancellations between poles and zeroes as well as by poles displacement outside the unit circle [15]. To achieve stability, a damping factor (r) must be included to force the poles and zeroes to be at a radius of r inside the unit circle. Then, the intrinsically stable version of the SDFT is:

$$\widetilde{X}_k(n) = rW_N^k \widetilde{X}_k(n-1) - r^N x(n-N) + x(n) \tag{3}$$

where $\widetilde{X}_k(n)$ is the estimated DFT output coefficient. The z-domain transfer function for the estimated kth-bin of the SDFT is:

$$H_{SDFT}(z) = \frac{1 - r^N z^{-N}}{1 - rW_N^k z^{-1}} \tag{4}$$

While this system is numerically stable, it no longer computes the exact value of $X(k)$ in Eq. (1), since a small error is induced by the damping factor. This error can be reduced via a suitable choice of r. The stable SDFT filter is shown in Fig. 1(a). This algorithm is implemented as an IIR filter with a comb filter followed by a complex resonator. The comb filter forces the filter's transient response to be $N-1$ samples in length, so the output will not reach a steady state until the comb filter stores the new input signal waveform.

The number of multiplications required in the SDFT can be reduced by creating a new pole/zero pair in its $H_{SDFT}(z)$ system function. This is achieved by multiplying the numerator and denominator of $H_{SDFT}(z)$ in Eq. (4) by the factor $\left(1 - rW_N^{-k} z^{-1}\right)$ yielding:

$$H_{SGT}(z) = \frac{\left(1 - rW_N^{-k} z^{-1}\right)\left(1 - r^N z^{-N}\right)}{1 - 2r\cos\left(2\pi k/N\right) z^{-1} + r^2 z^{-2}} \tag{5}$$

where the subscript SGT means Sliding Goertzel Transform. Like SDFT filter, SGT implementation is also marginally stable since its poles reside on the z-domain unit circle. To mitigate the stability drawback, a damping factor r is used in Eq. (5), to move the singularities towards the inside of the unit circle, thus assuring the system stability.

The linear difference equations of this transformation are:

$$v(n) = C_1\, v(n-1) - C_2\, v(n-2) + x(n) - r^N x(n-N) \tag{6a}$$

$$\widetilde{X}_k(n) = v(n) - rW_N^k v(n-1) \tag{6b}$$

where $C_1 = 2r\cos(2\pi k/N)$ and $C_2 = r^2$. The block diagram description of SGT is shown in Fig. 1(b), where the Standard Goertzel filter preceded by a comb filter can be observed. The computational workload of SGT implementation is less than that of SDFT as it only has real coefficients in the feedback path. Therefore, for real-time processing involving spectral updates on a sample-by-sample basis, the SGT method requires fewer multipliers than SDFT does [16,9,8].

The use of a damping factor in SDFT and SGT guarantees stability, but the filters output is no longer exactly equal to the kth-bin of an N-point DFT in Eq. (1). The error is reduced by making r very close to (but less than) unity. Additionally, in [12], a technique that reduces this error and, like SDFT and SGT, computes the kth-bin of an N-point DFT using a simple recursive algorithm, is developed. This technique is a periodically-time-varying system designed to produce an $\widetilde{X}_k(n)$ output signal that is mathematically equivalent to $X(k)$ in Eq. (1) at every Nth time instant. At other time instants, the difference can be arbitrarily made smaller through the proper choice of the damping factor r. This algorithm has a simple recursive implementation that renders it useful for approximating Eq. (1):

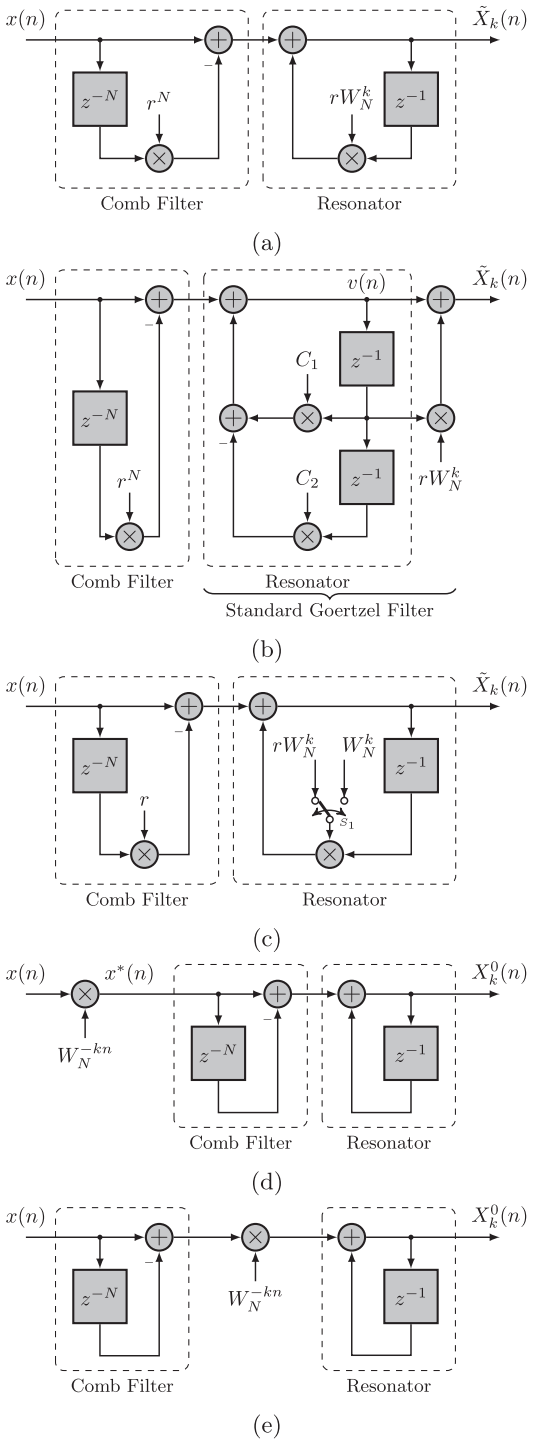

Fig. 1. Guaranteed-stable Sb-SDFT implementation as IIR filter. (a) SDFT. (b) SGT. (c) D&S algorithm. (d) mSDFT. (e) mSDFT, most efficient approach in Eq. (13).

$$\widetilde{X}_k(n) = \begin{cases} rW_N^k \widetilde{X}_k(n-1) - rx(n-N) + x(n), & (n \bmod N) = 0 \quad \text{(a)} \\ W_N^k \widetilde{X}_k(n-1) - rx(n-N) + x(n), & \text{otherwise.} \quad \text{(b)} \end{cases} \tag{7}$$

The algorithm described by Eq. (7) will be referred to as the Douglas and Soh (D&S) algorithm. The filter implementation of Eq. (7), shown in Fig. 1(c), requires two multiplications and two additions as well as the control logics to determine when $n \bmod N = 0$. In the figure, the change between Eq. (7a) and (7b) is performed by switch S_1. Therefore, the switching period of S_1 in Fig. 1(c) is equal to $N \times T_s$, where T_s is the sampling period, and its duty cycle is equal to one sample. It is worth mentioning that the effect of the nonlinear operation of D&S algorithm in the dynamic response is negligible as it only changes its structure every N samples.

There is a linear way of avoiding the reduction of accuracy generated by the damping factor, without compromising stability. SDFT implementation in Eq. (2) is marginally-stable, however for the particular case of $k = 0$ (DC component estimation), it takes the following form:

$$X_0(n) = [X_0(n-1) - x(n-N) + x(n)] \tag{8}$$

The absence of the W_N^k coefficient, which typically leads to stability issues when it is represented with finite precision, allows to implement the recursive expression without the damping factor r. Therefore, the recurrence in Eq. (8) is unconditionally stable and does not accumulate errors. The Modulated SDFT (mSDFT) algorithm uses the DFT modulation property to effectively shift the k component of an input signal to the position $k = 0$. This is accomplished by the multiplication of $x(n)$ by the modulation sequence W_N^{-kn}. This approach allows to exclude the complex twiddle factor from the resonator and avoid accumulated errors and potential instabilities [11]. The recursive realization of the mSDFT is:

$$X_k^0(n) = X_k^0(n-1) - x(n-N)W_N^{-k(n-N)} + x(n)W_N^{-kn} \tag{9}$$

where $X_k^0(n)$ is a complex constant related to the phase of the complex twiddle factor, since the modulation moves the desired kth-bin to $k = 0$ (zero Hz). The relation between the desired $X_k(n)$ and the computed $X_k^0(n)$ is:

$$X_k(n) = W_N^{kn} X_k^0(n) \tag{10}$$

It is worth noticing that if the application only requires DFT magnitude estimation, the complex multiplication in Eq. (10) is unnecessary because $|X_k^0|$ is equal to $|X(k)|$. The structure of mSDFT in Eq. (9) is depicted in Fig. 1(d). As there is no complex twiddle factor in the resonator, the singularities of mSDFT are precisely located (with no finite-precision numerical error) on the unit circle. Hence the accumulated errors and potential instabilities inherent of traditional Sb-SDFT algorithms are eliminated in mSDFT. In addition, the finite precision of the twiddle factor representation no longer constitutes a problem for being removed from the resonator loop. The trade-off for an improved accuracy and stability is a non-linear filter given the modulating sequence.

A z−domain transfer function for the kth-bin can be obtained by separating the effects of the modulation property in an auxiliary complex variable $(x^*(n))$.

$$x^*(n) = x(n)W_N^{-kn} \tag{11}$$

In Eq. (11), the chosen DFT bin with index k is shifted to the position $k = 0$. Once this occurs, the transfer function from x^* to X_k^0 becomes:

$$H_{DNF}(z) = \frac{X_k^0(z)}{x^*(z)} = \frac{1 - z^{-N}}{1 - z^{-1}} \tag{12}$$

Eq. (12) corresponds to a digital notch filter that rejects all the frequency multiples of f_s/N, being f_s the sampling frequency. Since $f_s = N \times f_o$, where f_o is the fundamental frequency of $x(n)$, the resulting transfer function has zeroes in all multiples of the input frequency. If multiple DFT frequency bins are to be computed, a comb filter is needed for each frequency bin. On the other hand, given the periodicity of W_N^{-kn}, as shown in [11], Eq. (9) can be rewritten as:

$$X_k^0(n) = X_k^0(n-1) + W_N^{-kn}[-x(n-N) + x(n)] \tag{13}$$

Whenever multiple DFT frequency bins are to be computed, equation Eq. (13) becomes a more efficient approach as only one comb filter is needed (Fig. 1). Also, it processes real values $(x(n))$ rather than complex ones $(x^*(n))$ as in the filter implementation of Eq. (9).

Table 1 shows a Sb-SDFT computational effort comparison for a real-only input with the use of a damping factor to ensure stability. It is worth noticing that the amount of operations reported for the mSDFT are those necessary for the computation of $X_k^0(n)$ instead of $X_k(n)$.

These methods have been applied in several works mainly for spectrum analysis and as filters stages [17–19], and the similarities between them have generally been disregarded. However, as they are derived from the conventional DFT, the equivalences between methods are discussed in the following sections.

3. Static analysis

It is common knowledge that the Cramer-Rao lower bound (CRLB) is an important performance limit which indicates the best estimation attainable with the available observations. CRLB assumes that the parameter is unknown but deterministic, and provides a lower bound on the variance of any unbiased estimation. A key feature of all estimation methods, in real applications, is immunity to noise in the acquired signal evaluated by its CRLB [20–22].

Computer simulations have been performed to evaluate the performance of SDFT, SGT, mSDFT and D&S algorithms for a single real sinusoid polluted with white Gaussian noise:

$$x(n) = A\cos(\omega n + \phi) + wgn(n) \tag{14}$$

where A and ϕ are the amplitude and initial phase, respectively, n is the time domain index, ω denotes the normalized angular frequency $(\omega = 2\pi f_o/f_s)$ and $wgn(n)$ is a zero-mean white Gaussian noise of variance σ_n^2. Under

Table 1
Sb-SDFT computational effort comparison, for real input.

Sb-SDFT		Single computation ($n = n_o$)		Next computation ($n = n_o + 1$)	
		Real multiplications	Real adds	Real multiplications	Real adds
SDFT	Eq. (3)	$5N$	$4N$	5	4
SGT	Eq. (6)	$3N + 2$	$3N + 1$	5	4
D&S	Eq. (7)	$5N$	$4N$	5	4
mSDFT	Eq. (13)	$2N$	$3N$	2	3

the assumption of white Gaussian noise, the CRLB for amplitude estimation is approximated by [23,24]:

$$CRLB_A = \frac{2\sigma_n^2}{N} \tag{15}$$

Parameters were assigned to $A = 1$, $f_o = 50$ Hz, $f_s = 6.4$ kHz, $N = 128$ and ϕ is a constant uniformly distributed between $[0, 2\pi)$. The signal-to-noise ratio is $SNR = A^2/(2\sigma_n^2)$, whereas different SNR levels were obtained by properly scaling the noise variance σ_n^2. All simulation results provided are the averages of 1000 independent runs. The damping factor was fixed at $r = 0.9999$ for SDFT, SGT, and D&S algorithm.

Fig. 2 shows variance in the estimate of A ($\sigma_{\widehat{A}}$) versus SNR. It can be seen that $SNR = -10$ dB is the threshold level below which variance rapidly worsens. From this threshold, $\sigma_{\widehat{A}}$ is below CRLB for all the methods, which means that the results no longer correspond to an efficient unbiased estimator.

When SNR is between the threshold level and 30 dB the four methods exhibit similar behavior, being over CRLB. From this SNR level, the $\sigma_{\widehat{A}}$ for SDFT and SGT does no longer converge to CRLB and asymptotically approaches the -63 dB bound. This is attributed to the fact that the error introduced by the damping factor in Eq. (3) and Eq. (6) is more significant than the effect of SNR level. The same applies to the D&S algorithm, but starting at $SNR = 60$ dB. For increasing SNR levels, the D&S algorithm approaches the -91 dB bound. Hence, it can be concluded that D&S algorithm, compared to SDFT and SGT, extends the range in which it can be considered as an efficient unbiased estimator at the expense of a slightly increased computational cost and a non-linear operation. For the range of SNR levels shown in Fig. 2, the variance of $\widehat{A}$ computed by the mSDFT remains on CRLB curve, due to the absence of a damping factor.

The $\sigma_{\widehat{A}}$ versus N at $SNR = 30$ dB are illustrated in Fig. 3. As expected, N increase, i.e., the length of the sliding window, reduces the variance of $\widehat{A}$ in the four methods. This is mainly because the estimations are computed in a larger sliding time window, i.e., more samples are used for the estimation.

Finally, the effect of the damping factor on the $\sigma_{\widehat{A}}$ is shown in Fig. 4. The simulation is performed for $SNR = 80$ dB because at this level SDFT, SGT and D&S

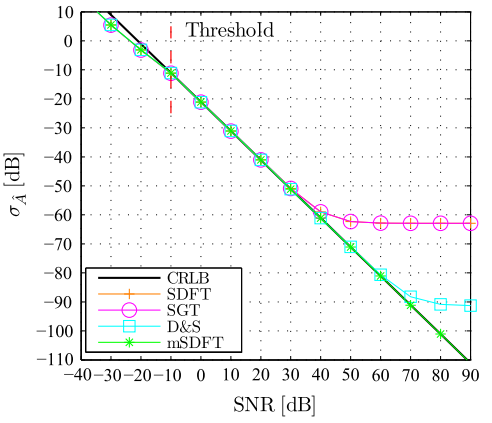

Fig. 2. Variance of $\widehat{A}$ versus SNR levels for the analyzed estimators with $r = 0.9999$ and $N = 128$.

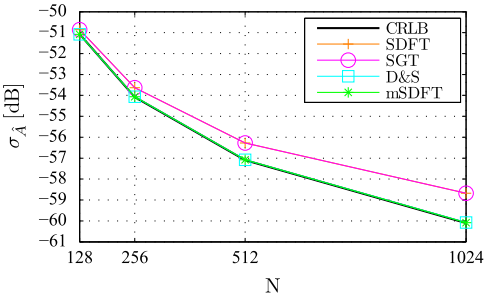

Fig. 3. Variance of $\widehat{A}$ versus N for the four estimators, with $r = 0.9999$ and $SNR = 30$ dB.

algorithms do not lie on CRLB curve and have converged to their final values listed in Fig. 2. Since mSDFT is independent from r, its $\sigma_{\widehat{A}}$ remains constant and equal to CRLB for this simulation. Fig. 4 shows that when $r \longrightarrow 1$, the $\sigma_{\widehat{A}}$ for SDFT, SGT and D&S algorithm approaches CRLB. This is valid for any SNR after the threshold. An interesting corollary to this analysis is that for the ideal case ($r = 1$), i.e., an infinite word precision case, with SNR levels beyond the threshold, the curves of SDFT, SGT, D&S and mSDFT algorithms lay over CRLB and provide an identical static performance.

4. Dynamic behavior

In this section, dynamic responses of Sb-SDFT methods are analyzed. For this study, the following test signal with significant harmonic content was adopted:

$$\begin{aligned} x(n) = {} & A \cdot 1.0 \cos(\omega n + \phi_1) + A \cdot 0.2 \cos(3\omega n + \phi_3) \\ & + A \cdot 0.1 \cos(5\omega n + \phi_5) + A \cdot 0.04 \cos(7\omega n + \phi_7) \\ & + A \cdot 0.08 \cos(9\omega n + \phi_9) + A \cdot 0.06 \cos(11\omega n + \phi_{11}) \\ & + A \cdot 0.03 \cos(13\omega n + \phi_{13}) \end{aligned} \tag{16}$$

where the normalized frequency is the same as that used for the static analysis, $A = 1$ and $\phi_i = \{0°, 180°, 0°, 0°,$

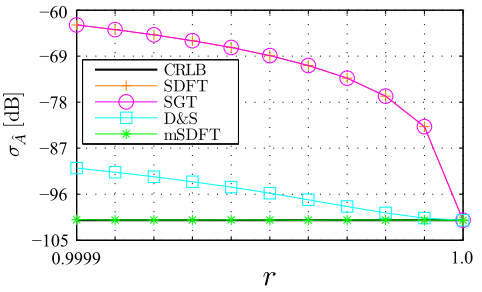

Fig. 4. Variance of $\widehat{A}$ versus r for the four estimators at $SNR = 80$ dB.

$180°, 180°, 180°\}$ are the initial phases of the harmonics of order *i*. The selected signal is rich in odd harmonic content for being the most usual case. The damping factor is set at $r = 0.9999$, for SDFT, SGT, and D&S algorithm.

In Fig. 5, the estimated amplitude of the fundamental component $(\widehat{A}_1)$ for all the algorithms can be observed (the estimated values exhibited correspond to the steady-state). The reference value is displayed with a black dashed line. SDFT and SGT have the same steady-state error resulting from the use of a damping factor. This error has a mean value with an overlaid ripple that is a direct consequence of the use of the stable versions of IIR filters Eqs. (4) and (5), that do not provide infinite rejection to the undesired harmonics of the input signal. The D&S algorithm significantly reduces error and maintains the same damping factor than the two previous cases, resulting in improved system performance. In Fig. 5, it is shown that when $(n \bmod N) = 0$, the estimation is accurate, which is consistent with the period of the fundamental component of the test signal. On the other hand, mSDFT provides precise estimation of the amplitude, since it does not require a damping factor to ensure stability.

Fig. 6 displays the dynamic response of the algorithms to a sudden amplitude step of 20%. This figure reveals that all the algorithms yield the same dynamic response during the transient, disregarding the differences from the damping factor effect, which are more apparent in SDFT and SGT. For all cases, the duration of the transient response is equal to the length of the sliding window. From the studies, it can be concluded that mSDFT is the most accurate algorithm of all the Sb-SDFT analyzed.

5. Single-bin Sliding DFT frequency adaptation

The Sb-SDFT implementations analyzed in this paper suffer the same problem when working with non-stationary signals such as voltages and currents from the mains. If the analyzed sequence does not correspond exactly to an integer number of cycles of the signal, inaccuracies arise due to the spectral leakage and picket-fence effect. There are two typical strategies for mitigating these errors. The first one is to weigh the sequence data with a window and keep a fixed sampling frequency. This option increases the computational cost and does not take advantage of the recursive implementation of Sb-SDFT. The second strategy consists in adapting the sampling frequency to a multiple

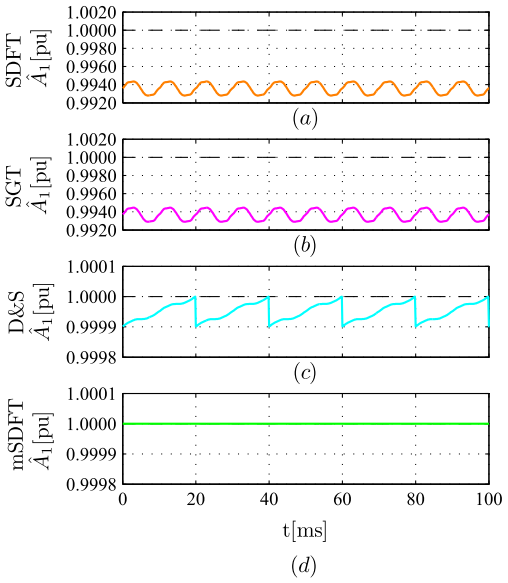

Fig. 5. Amplitude estimation of the fundamental component (A_1) in steady state using the selected Sb-SDFT algorithms.

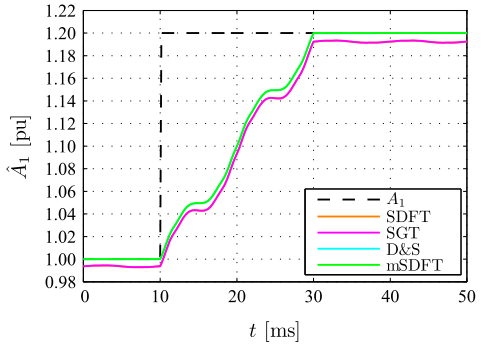

Fig. 6. Transient for the estimation of A_1, when the test signal is undergoing a 20% step-change in its harmonic amplitude for the selected Sb-SDFT algorithms.

of the line frequency. This ensures that the filter is tuned to the fundamental frequency, which allows following its variations. This approach takes advantage of the recursive nature of Sb-SDFT at a low computational cost and allows optimal operation of the system.

The variable sampling period approach was developed by the authors to design synchronization methods [25–27]. Yet its usefulness goes beyond this application. This technique has recently been adapted to dynamically adjust the sampling frequency in a harmonic measurement method based on mSDFT [14].

In this section, the proposal in [14] is generalized so as to be used with any Sb-SDFT implementation. The technique of variable sampling period is briefly described and the way in which it can be adapted to be used in a scheme of harmonics measurement is discussed. A unified small-signal model, which allows to extend the results obtained

to any Sb-SDFT is also developed. This model is valid for any application using this type of transformation within a control loop governed by phase differences. The system controller is designed based on this model and depending on the application requirements.

5.1. Variable Sampling Period Technique (VSPT)

VSPT allows to adapt the sampling frequency to be N times the grid frequency. This technique has proven to be efficient both in three-phase and in single-phase applications yielding a robust synchronization mechanism, whose effectiveness has been tested under different conditions and scenarios [25–27].

Fig. 7 illustrates the basic VSPT scheme for single-phase implementation. The operating principle is based on the dynamic adjustment of the sampling frequency. The input signal is sampled and the input phase ($(\varphi_u(n))$) is extracted by the phase detector. Concomitantly with the input sampling, the Reference Generator provides a signal called reference phase:

$$\varphi_{ref}(n) = \frac{2\pi n}{N} \tag{17}$$

The method relies on sampling period modification, so as to achieve a null error signal ($(e_\varphi(n))$) between $\varphi_{ref}(n)$ and $\varphi_u(n)$. This is achieved by varying the sampling period $T_S(n)$ as a function of the phase error by means of the controller $G_c(z)$. With each new sampling period, the Sampling Generator produces a clock signal (CLK) that starts the conversion and increments the reference phase. The implementation of the phase detector and phase error calculation, enclosed by dashed lines in Fig. 7, is key for the proper functioning of this technique. In [14], it was implemented as one single component, by taking advantage of mSDFT attributes.

5.2. Single-bin SDFT small-signal model

VSPT allows to adapt the sampling rate to a multiple of the grid frequency, thus avoiding the problems concerning DFT when working with non-stationary signals. In order to adapt the sampling period, an error signal is needed, which is related to the phase difference between the fundamental component of the input signal and the reference phase. This phase error allows to implement a closed-loop control of the sampling period to attain synchronization. To generalize this proposal to any Sb-SDFT, a general model should be devised. The purpose of obtaining a unified model is to make the choice of an Sb-SDFT independent from the design of the control in charge of frequency adjustment, rendering the design and implementation process more flexible and convenient. It also allows to change the algorithm with no need to redesign the adopted control.

The real and imaginary components of $X_k(n)$ are the in-phase and in-quadrature components of the desired kth-bin, respectively. This is true for the $\widetilde{X}_k(n)$ obtained with SDFT, SGT and D&S algorithm, but does not apply to the $X_k^0(n)$ obtained with mSDFT, unless Eq. (10) is used to obtain $X_k(n)$, which increases computational cost. In [14], it was shown that the use of Eq. (10) is completely unnecessary for VSPT implementation.

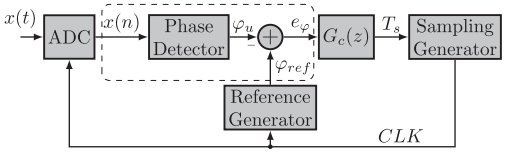

Fig. 7. Scheme of Variable Sampling Period Technique (VSPT) for single-phase.

As mentioned in Section 2–4, when $r \longrightarrow 1$ and for a real input signal, SDFT, SGT and D&S algorithms become equivalent. Therefore, for this scenario and for small-signal conditions, these three filters supply the same in-phase and in-quadrature components, which can be expressed as follows:

$$\begin{cases} \mathrm{Re}\{\widetilde{X}_k(n)\} = \frac{\widehat{A}_k N}{2}\cos(k\hat{\varphi}_u(n) + \hat{\phi}_k) & \text{(a)} \\ \mathrm{Im}\{\widetilde{X}_k(n)\} = \frac{\widehat{A}_k N}{2}\sin(k\hat{\varphi}_u(n) + \hat{\phi}_k) & \text{(b)} \end{cases} \tag{18}$$

where $\hat{\varphi}_u(n)$ is the estimated phase of the input signal, $\widehat{A}_k$ and $\hat{\phi}_k$ are the estimated amplitude and initial phase, respectively, for the kth-bin of an N-point DFT. In several applications (including VSPT), the estimation of the fundamental component of a given electrical signal is crucial for its proper functioning. Therefore, the fundamental component $(k = 1)$ is taken as the system reference and $\phi_1 = 0^\circ$ is adopted, which results in

$$\begin{cases} \mathrm{Re}\{\widetilde{X}_k(n)\} = \frac{\widehat{A}_1 N}{2}\cos(\hat{\varphi}_u(n)) & \text{(a)} \\ \mathrm{Im}\{\widetilde{X}_k(n)\} = \frac{\widehat{A}_k N}{2}\sin(\hat{\varphi}_u(n)) & \text{(b)} \end{cases} \tag{19}$$

From Eq. (19), the estimated phase of the input signal can be recovered as:

$$\hat{\varphi}_u(n) = angle(\widetilde{X}_1(n)) \tag{20}$$

and the phase error between the incoming signal and the system reference phase is:

$$\tilde{e}_\varphi(n) = \varphi_{ref}(n) - \hat{\varphi}_u(n) \tag{21}$$

Fig. 8(a) displays the scheme for phase error estimation, based on Eqs. (19)–(21). This scheme is equivalent to the portion enclosed by dashed line in the VSPT scheme in Fig. 7.

A slightly different case is that of mSDFT, because $X_k^0 \neq X_k$ (Eqs. (13) and (10)). In [14], it is shown that mSDFT output (Fig. 13(d) and (e)) is:

$$\begin{cases} \mathrm{Re}\{X_k^0(n)\} = \frac{A_k N}{2}\cos(k\varphi_{ref}(n) - k\varphi_u(n) - \phi_k) & \text{(a)} \\ \mathrm{Im}\{X_k^0(n)\} = \frac{A_k N}{2}\sin(k\varphi_{ref}(n) - k\varphi_u(n) - \phi_k) & \text{(b)} \end{cases} \tag{22}$$

By setting $k = 1$, taking $\phi_1 = 0^\circ$ and assuming that the phase difference between $\varphi_{ref}(n)$ and $\varphi_u(n)$ is small, (22) can be approximated by:

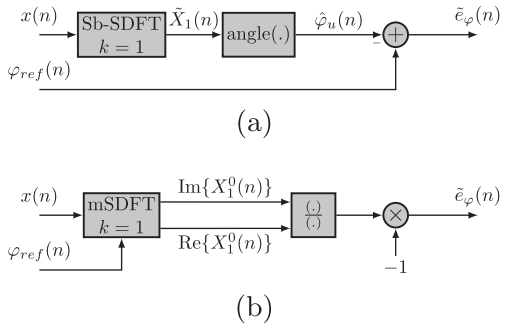

Fig. 8. (a) Phase error estimation scheme based on Sb-SDFT (except for mSDFT). (b) Phase error estimation scheme based on mSDFT.

$$\begin{cases} \mathrm{Re}\{X_1^0(n)\} = \frac{A_1 N}{2} & \text{(a)} \\ \mathrm{Im}\{X_1^0(n)\} = \frac{A_1 N}{2}(\varphi_{ref}(n) - \varphi_u(n)) & \text{(b)} \end{cases} \tag{23}$$

As seen in Eq. (23), the real component of X_1^0 is proportional to A_1 and the imaginary component is proportional to A_1 and the phase difference. Therefore, by normalizing the imaginary component, the phase error may be estimated by:

$$\tilde{e}_\varphi(n) = -\frac{\mathrm{Im}\left\{X_1^0(n)\right\}}{\mathrm{Re}\left\{X_1^0(n)\right\}} = \varphi_{ref}(n) - \varphi_u(n) \tag{24}$$

Fig. 8(b) shows the scheme for phase error estimation with mSDFT, based on Eqs. (23) and (24). Fig. 8(b) is equivalent to the portion enclosed by the dashed line in the VSPT scheme in Fig. 7.

Since all the Sb-SDFT methods evaluated in this work derive from Eq. (1), they are mathematically equivalent, and the system phase error ($e_\varphi(n)$) for small deviation is approximately equal. Therefore, a simplified model can be extrapolated for the phase error signal, regardless of the algorithm used. The model is conveniently made from mSDFT as its transfer function in the z-domain is the most simple of all, as it has no coefficients Eq. (12). This is explained by the fact that all implementations of Sb-SDFT result from applying properties and mathematical operations to Eq. (1), all of which can be modeled from the normalized mSDFT. The small signal model for all Sb-SDFTs governed by the phase differences is presented in Fig. 9.

5.3. Controller design

In [14], the mathematical modeling of VSPT is detailed, together with the controller design for a harmonics measurement method based on mSDFT. This method uses the imaginary component of X_1^0 as a phase error signal. As shown in Eq. (23b), amplitude A_1 is part of the control loop gain of the sampling period. As a consequence, the dynamic response of this system may be compromised in certain scenarios, e.g., if large variations in the input signal amplitude occur.

Starting from the unified model discussed in Section 5.2, a control design methodology similar to that used in [14] is analyzed. All the Sb-SDFT methods reviewed

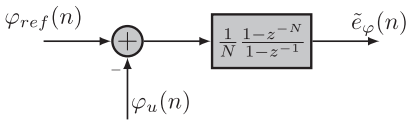

Fig. 9. Unified small-signal system model.

can be adjusted using the normalized error signal given by Eq. (24) and the unified small-signal model (Fig. 9), obtaining the mathematical model shown in Fig. 10. The specifications and requirements to be met by the controller ($G_c(z)$) are determined by the application.

In the common practice, there are two typical set of requirements to be considered when designing $G_c(z)$. Certain applications require zero phase error and frequency synchronization for normal operation. In these cases, the controller must be proportional-integral to achieve zero phase error in steady-state, the resulting system being a type II system. Other applications only require frequency synchronization, which reduces the restrictions on the controller design, resulting in a faster and improved dynamic response. In these applications, a proportional controller suffices, the resulting system being a type I system.

The transfer functions for both controllers in the z-domain are:

$$G_P(z) = K_P \tag{25}$$

$$G_{PI}(z) = K_{PI}\frac{z - a_{PI}}{z - 1} \tag{26}$$

As an example of design, $\bar{\omega} = 2\pi \times 50\ \mathrm{rad/s}$ and $N = 128$ are adopted. Concerning dynamics, a phase margin of 45° and maximum bandwidth are adopted as design criteria for $G_c(z)$. Based on this, and using the design methodology proposed in [14], the parameters of the controller are $K_P = 4.3408 \cdot 10^{-5}$, $K_{PI} = 1.7304 \cdot 10^{-5}$ and $a_{PI} = 0.9974$. The bandwidth obtained for $G_P(z)$ and $G_{PI}(z)$ are 12.505 Hz and 5.905 Hz, respectively.

To evaluate the performance of both controllers, a simulation was performed. In view of the similarity in the small-signal characteristics of the different methods, which is validated in the experimental results section, their dynamic behaviors will be similar as well. Hence, only the simulation results obtained with the mSDFT method are presented. This simulation used Eq. (16) as a test signal, with the same values used in Section 4 for a system composed of a mSDFT tuned with $k = 1$ and with a VSPT based on the model shown in Fig. 10. Fig. 11 compares the system dynamic response to different disturbances for both controllers.

The figure presents the estimated amplitude of the fundamental component ($\hat{A}_1$), the estimated and real fundamental input frequency ($\hat{f}_o$ and f_o, respectively) and the phase error (e_φ) for both controllers. To begin with, the effect of an amplitude step change in the test signal was evaluated. The signal was increased to 20% of the nominal value at $t = 0.5$ s. The estimation of A_1 falls into the 1% band in 20 ms for both controllers with a null steady

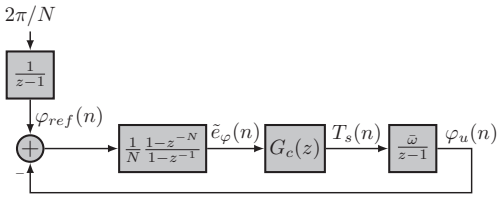

Fig. 10. System model for Sb-SDFT frequency adjustment based on VSPT.

state error. During this disturbance, the phase error and the estimated frequency, for both systems, were slightly affected.

The ability of the method to measure harmonics in situations where the frequency deviates from its nominal value was evaluated by simulating two possible scenarios. The first simulation analyzed the effect of a frequency step of 0.5 Hz at $t = 1.0$ s. The aim of the second simulated scenario, in turn,was to verify the method performance when continuous frequency variation occurred. To this end, the fundamental frequency varied at a rate of 0.5 Hz/s from $t = 2$ s to $t = 3$ s. Regarding the frequency step, the type I system responded slightly faster as compared to the type II system. In addition, a constant phase error was observed with the proportional controllers. On the other hand, as regards the frequency ramp, the type II system delivered best performance, since it had better tracking of the frequency ramp. Importantly, in both scenarios and for both controls, amplitude estimation was not compromised.

6. Experimental validation

This section concentrates on the experimental results for the implementation of the reviewed Sb-SDFT with VSPT. The experimental setup comprised a fixed-point DSP TMS320F2812 (32bits, 150 MHz) and an A/D converter board with an ADS8568 (eight 16-bit A/D channels and 2 μs conversion time). The algorithms were tuned as described in the previous section with $N = 128$, $r = 0.9999$ (for SDFT and SGT), $r = 0.995$ (for the D&S algorithm) and the proportional-integral controller given by Eq. (26) was adopted. Due to the non-linear operation of the D&S algorithm, a smaller r was used to ensure stability while preserving the same word length used in the other methods. In order to evaluate the methods performance, other DSP was used to generate the test signals.

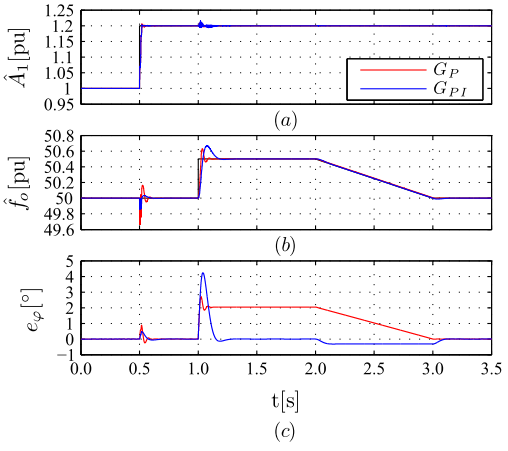

Fig. 11. Comparison between the closed loop response of Sb-SDFT algorithm with two different controllers: (a) accuracy in the estimation of A_1, (b) ability to track f_o and (c) system phase error.

6.1. Harmonic distortion

Fig. 12 shows the performances of all the methods when a clean 9V input signal witha nominal frequency equal to 50 Hz change to Eq. (16) with $A = 8V$ and the same ϕ_i used in Section 4. Fig. 12(a) illustrates the input signal and the estimated amplitude of the fundamental component $(\widehat{A}_1)$ computed by all methods. In addition, reference amplitude is presented in dashed line. As expected, the transient is equal to one period of the test signal, i.e., it is the time it takes the comb filter to store the new input sequence for all Sb-SDFTs. The dynamics of the Sb-SDFT both in steady state and during the transient is consistent with that reported in previous sections. To highlight this, a detail of $\widehat{A}_1$ in steady state is provided in Fig. 12(b). mSDFT is the most accurate of all, as expected. However, as opposed to the simulations shown in Section 4, the amplitude of D&S algorithm ripple in steady state is similar to the amplitude of SDFT and SGT ripple error. This is ascribed to the fact that a minor damping factor was required in the D&S algorithm in order to ensure stability in DSP implementation, resulting in lower performance as compared to the theoretical analysis. The adjustment of the sampling period $(\widehat{T}_s)$ obtained with each method is shown in Fig. 12(c), where the reference value for a fundamental frequency of 50 Hz (156.250 μs) is highlighted in black dashed lines. The temporal evolution of $\widehat{T}_s$ is identical for all the methods which is agreement with the theoretical study performed in this paper and validates the proposed small-signal model. Table 2 summarizes the performance of all the methods in steady state under both clean and distorted conditions.

6.2. Frequency variation

The ability of Sb-SDFT with VSPT to track the grid frequency variations is shown in Fig. 13. The fundamental frequency is varied at a rate of 10 Hz/s from 51 Hz to 49 Hz, for a clean input signal with an amplitude of 9 V. Then a frequency step of 2 Hz returns the fundamental frequency to 51 Hz. Table 2 shows the $\widehat{T}_s$ in steady state, where 153.186 μs and 159.438 μs are the ideal sampling period corresponding to 51 Hz and 49 Hz, respectively. Fig. 13(c) displays how the sampling period is adjusted to track the frequency variations and thus mitigate the pitfalls of the DFT-based algorithms when working with non-stationary signals. The estimation of A_1 for this variation frequency is shown in Fig. 13(a), where the reference amplitude is indicated by a dashed black line. A detail is shown in Fig. 13(b), where a similar behavior is observed and differences are given only by the precision of each Sb-SDFT

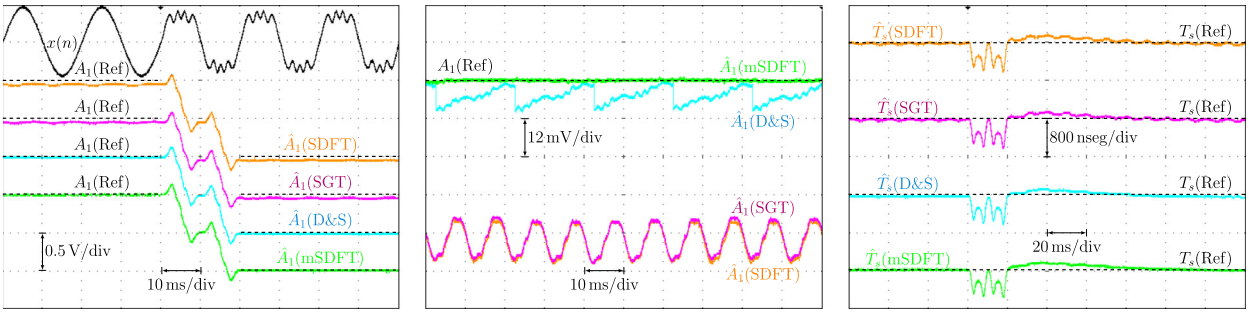

Fig. 12. Systems performance in a grid polluted with harmonic distortion. (a) Input signal and estimation of A_1. (b) Details of the estimation of A_1, after the perturbation occurs. (c) Adaptive sampling period.

Table 2
Measurement comparative.

$x(t)$	Reference	SDFT		SGT		D&S		mSDFT	
		μ	σ	μ	σ	μ	σ	μ	σ
Ideal (f_o = 50 Hz)									
$\hat{V}_1$ (V)	9	8.934	$4.23 \cdot 10^{-5}$	8.935	$4.24 \cdot 10^{-5}$	8.985	$8.51 \cdot 10^{-6}$	8.991	$1.58 \cdot 10^{-7}$
$\hat{T}_s$ (s)	$156.25 \cdot 10^{-6}$	$156.243 \cdot 10^{-6}$	$1.63 \cdot 10^{-16}$	$156.243 \cdot 10^{-6}$	$1.64 \cdot 10^{-16}$	$156.243 \cdot 10^{-6}$	$9.94 \cdot 10^{-18}$	$156.240 \cdot 10^{-6}$	$1.95 \cdot 10^{-18}$
Distorted (f_o = 50 Hz)									
$\hat{V}_1$ (V)	8	7.939	$2.14 \cdot 10^{-5}$	7.941	$2.15 \cdot 10^{-5}$	7.989	$6.69 \cdot 10^{-6}$	7.991	$1.10 \cdot 10^{-7}$
$\hat{T}_s$ (s)	$156.25 \cdot 10^{-6}$	$156.256 \cdot 10^{-6}$	$2.45 \cdot 10^{-16}$	$156.243 \cdot 10^{-6}$	$2.45 \cdot 10^{-16}$	$156.243 \cdot 10^{-6}$	$1.91 \cdot 10^{-17}$	$156.253 \cdot 10^{-6}$	$1.87 \cdot 10^{-18}$
Ideal (f_o = 51 Hz)									
$\hat{V}_1$ (V)	9	8.936	$4.24 \cdot 10^{-5}$	8.938	$4.25 \cdot 10^{-5}$	8.988	$9.08 \cdot 10^{-6}$	8.993	$1.79 \cdot 10^{-7}$
$\hat{T}_s$ (s)	$153.186 \cdot 10^{-6}$	$153.193 \cdot 10^{-6}$	$1.63 \cdot 10^{-16}$	$153.193 \cdot 10^{-6}$	$1.64 \cdot 10^{-16}$	$153.193 \cdot 10^{-6}$	$9.85 \cdot 10^{-18}$	$153.191 \cdot 10^{-6}$	$2.60 \cdot 10^{-18}$
Ideal (f_o = 49 Hz)									
$\hat{V}_1$ (V)	9	8.934	$4.25 \cdot 10^{-5}$	8.936	$4.25 \cdot 10^{-5}$	8.986	$8.93 \cdot 10^{-6}$	8.991	$2.89 \cdot 10^{-7}$
$\hat{T}_s$ (s)	$159.438 \cdot 10^{-6}$	$159.445 \cdot 10^{-6}$	$1.65 \cdot 10^{-16}$	$159.445 \cdot 10^{-6}$	$1.65 \cdot 10^{-16}$	$159.445 \cdot 10^{-6}$	$1.01 \cdot 10^{-17}$	$159.442 \cdot 10^{-6}$	$7.17 \cdot 10^{-19}$

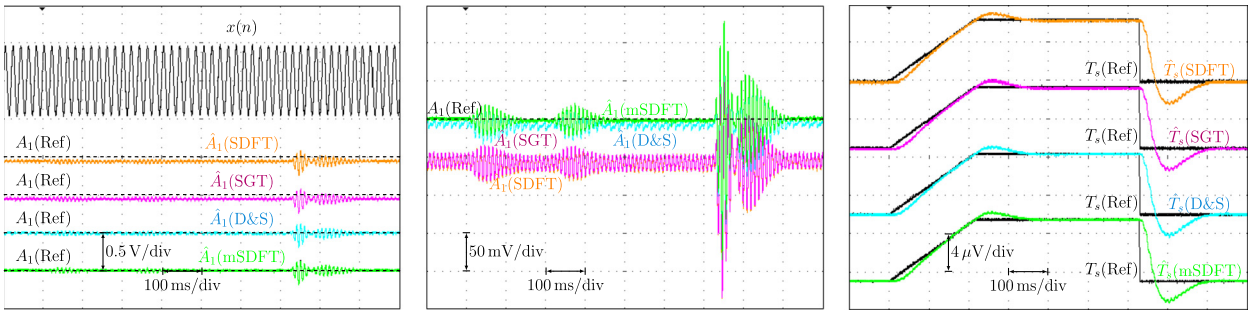

Fig. 13. Systems performance under frequency variation condition. (a) Input signal and estimation of A_1. (b) Details of the estimation of A_1. (c) Adaptive sampling period.

algorithm. Table 2 summarizes the performance of all the methods in steady state.

7. Conclusions

In this work, a comparative study of four Sb-SDFT algorithms is conducted. The comparison includes: filter structure, static analysis, dynamic behavior and implementation issues on finite word-length precision systems. Based on theoretical studies as well as on simulation and experimental results, it is concluded that all these methods are equivalent, since they are all derived from the conventional DFT, and so they can be indistinctly adopted for many applications.

As far as disturbance rejection and precision on spectral estimation are concerned, this work shows that SDFT and SGT are identical and that no differences are observed. On the other hand, the D&S algorithm increases performance accuracy in comparison to the previously mentioned methods. An interesting issue related to this method is that a lower damping factor, as compared to SDFT and SGT, had to be adopted to ensure stability. As a result, the mean error was reduced in spectral estimation but the ripple error was similar for the three methods. SDFT and SGT are widely used due to their simple and straightforward implementation, at the expense of an error in precision attributed mainly to the use of a damping factor. In applications requiring greater precision, this error can be mitigated by using the D&S algorithm. Moreover, it can be eliminated by using mSDFT due to the absence of such damping factor, resulting in better performance. The results of the study have shown that mSDFT is the best option when it comes to precision and noise rejection. However, this method is the less frequently used due to its non-linear characteristic.

Regardless of the Sb-SDFT method adopted, grid synchronization becomes essential for obtaining a proper response in terms of accuracy and speed. In this sense, VSPT allows to obtain a sampling frequency synchronized to the grid frequency. However, since it is a closed-loop method, a model of the system is required. This work proposes a unified small-signal system model, which was used to design a generic adaptive frequency loop. This frequency adaptive loop is based on VSPT and allows to mitigate spectral leakage and picket-fence effects, common pitfalls in any DFT-based algorithm. As a consequence, developers can design the adaptive frequency loop regardless of the Sb-SDFT method adopted, with the possibility of changing it depending on the precision required by the application.

Acknowledgement

This work was supported by the Consejo Nacional de Investigaciones Científicas y Técnicas, Argentina, by the Universidad Nacional de Mar del Plata, Argentina, by the Ministerio de Ciencia, Tecnología e Innovación Productiva, Argentina and the Agencia Nacional de Promoción Científica y Tecnológica, Argentina.

References

[1] M. Bollen, I. Gu, Signal Processing of Power Quality Disturbances, Wiley-IEEE Press, 2006.
[2] S. Chattopadhyay, Electric Power Quality, Power Systems, Springer, London, Limited, 2011.
[3] J. Arrillaga, N. Watson, Power System Harmonics, Wiley, 2003.
[4] A.V. Oppenheim, R.W. Schafer, J.R. Buck, Discrete-Time Signal Processing, second ed., Prentice Hall, 1999.
[5] E.O. Brigham, The Fast Fourier Transform and Its Applications, Prentice-Hall Inc., Upper Saddle River, NJ, USA, 1988.
[6] J.W. Cooley, J.W. Tukey, An algorithm for the machine calculation of complex fourier series, Math. Comput. 19 (90) (1965) 297–301.
[7] R.I. Hartley, K. Welles, Recursive computation of the fourier transform, in: IEEE International Symposium on Circuits and Systems, 1990, vol. 3, 1990, pp. 1792–1795. http://dx.doi.org/10.1109/ISCAS.1990.111983.
[8] E. Jacobsen, R. Lyons, The sliding dft, IEEE Signal Process. Mag. 20 (2) (2003) 74–80, http://dx.doi.org/10.1109/MSP.2003.1184347.
[9] J.F. Chicharo, M.T. Kilani, A sliding goertzel algorithm, Signal Process. 52 (1996) 283–297.
[10] R. Lyons, Streamlining Digital Signal Processing: A Tricks of the Trade Guidebook, second ed., Wiley-IEEE Press, 2007.
[11] K. Duda, Accurate, guaranteed stable, sliding discrete fourier transform [dsp tips amp; tricks], IEEE Signal Process. Mag. 27 (6) (2010) 124–127, http://dx.doi.org/10.1109/MSP.2010.938088.
[12] S. Douglas, J. Soh, A numerically-stable sliding-window estimator and its application to adaptive filters, in: Conference Record of the Thirty-First Asilomar Conference on Signals, Systems & Computers, 1997, vol. 1, 1997, pp. 111–115. http://dx.doi.org/10.1109/ACSSC.1997.680039.
[13] A. Girgis, F. Ham, A quantitative study of pitfalls in the fft, IEEE Trans. Aerospace Electron. Syst. AES-16 (4) (1980) 434–439, http://dx.doi.org/10.1109/TAES.1980.308971.
[14] C. Orallo, I. Carugati, S. Maestri, P. Donato, D. Carrica, M. Benedetti, Harmonics measurement with a modulated sliding discrete fourier transform algorithm, IEEE Trans. Instrum. Measur. 63 (4) (2014) 781–793, http://dx.doi.org/10.1109/TIM.2013.2287801.
[15] J.-H. Kim, T.-G. Chang, Analytic derivation of the finite wordlength effect of the twiddle factors in recursive implementation of the sliding-dft, IEEE Trans. Signal Process. 48 (5) (2000) 1485–1488, http://dx.doi.org/10.1109/78.839998.
[16] G. Goertzel, An algorithm for the evaluation of finite trigonometric series, Am. Math. Monthly 65 (1) (1958) 34–35.
[17] J. Alfonso-Gil, S. Orts-Grau, N. Muñoz-Galeano, F. Gimeno-Sales, S. Segui-Chilet, Measurement system for a power quality improvement structure based on ieee std.1459, IEEE Trans. Instrum. Measur. 62 (12) (2013) 3177–3188, http://dx.doi.org/10.1109/TIM.2013.2270901.
[18] S. Mishra, D. Das, R. Kumar, P. Sumathi, A power-line interference canceler based on sliding dft phase locking scheme for ecg signals, IEEE Trans. Instrum. Measur. PP (99) (2014), http://dx.doi.org/10.1109/TIM.2014.2335920. pp. 1-1.
[19] P. Sumathi, P. Janakiraman, Sdft-based ultrasonic range finder using am continuous wave and online parameter estimation, IEEE Trans. Instrum. Measur. 59 (8) (2010) 1994–2004, http://dx.doi.org/10.1109/TIM.2009.2032881.
[20] S.M. Kay, Fundamentals of Statistical Signal Processing: Estimation Theory, first ed., Prentice-Hall PTR, 2010.
[21] D. Rife, R. Boorstyn, Single tone parameter estimation from discrete-time observations, IEEE Trans. Inform. Theory 20 (5) (1974) 591–598, http://dx.doi.org/10.1109/TIT.1974.1055282.
[22] D.C. Rife, R.R. Boorstyn, Multiple tone parameter estimation from discrete-time observations, Bell Syst. Tech. J. 55 (9) (1976) 1389–1410, http://dx.doi.org/10.1002/j.1538-7305.1976.tb02941.x.
[23] T. Andersson, P. Handel, Ieee standard 1057, cramer-rao bound and the parsimony principle, IEEE Trans. Instrum. Measur. 55 (1) (2006) 44–53, http://dx.doi.org/10.1109/TIM.2005.861497.
[24] P. Handel, Parameter estimation employing a dual-channel sine-wave model under a gaussian assumption, IEEE Trans. Instrum. Measur. 57 (8) (2008) 1661–1669, http://dx.doi.org/10.1109/TIM.2008.923782.
[25] S. Maestri, P. Donato, R. Petrocelli, I. Carugati, D. Carrica, M. Benedetti, Synchronization method for three phase applications, Int. Rev. Electr. Eng. (IREE) 5 (4) (2010) 1728–1735. Praise Worthy Prize (Italia).
[26] I. Carugati, S. Maestri, P. Donato, D. Carrica, M. Benedetti, Variable sampling period filter pll for distorted three-phase systems, IEEE Trans. Power Electron. 27 (1) (2012) 321–330, http://dx.doi.org/10.1109/TPEL.2011.2149542.
[27] I. Carugati, P. Donato, S. Maestri, D. Carrica, M. Benedetti, Frequency adaptive pll for polluted single-phase grids, IEEE Trans. Power Electron. 27 (5) (2012) 2396–2404, http://dx.doi.org/10.1109/TPEL.2011.2172000.